Hypocrellin-Loaded Gold Nanocages with High Two-Photon Efficiency for Photothermal/Photodynamic Cancer Therapy *in Vitro*

Liang Gao, Jinbo Fei, Jie Zhao, Hong Li, Yue Cui, and Junbai Li*

Beijing National Laboratory for Molecular Sciences (BNLMS), Key Lab of Colloid and Interface Science, Institute of Chemistry, Chinese Academy of Sciences, Beijing 100190, China

ABSTRACT A new bioconjugate nanostructure was constructed by using photosensitizer-incorporated mixed lipid-coated gold nanocages for two-photon photothermal/photodynamic cancer therapy *in vitro* with high efficiency. Scanning electron microscopic and transmission electron microscopic images reveal that the precursors and bioconjugate nanostructure as-prepared are narrowly dispersed and possess uniform morphologies. The relevant energy dispersion X-ray analysis and UV—vis spectra indicate that the bioconjugate nanostructure above was assembled successfully and has a strong absorption in the near-infrared region. Fluorescence and electronic spin resonance results show that the gold nanocage in the bioconjugate nanostructure can dramatically quench the photosensitizer and inhibit the production of singlet oxygen, which is supposed to alleviate the photosensitizers' unwanted side effects originating from their nontargeted distribution. We have demonstrated that as the nanocomplex is internalized by cancer cells, under two-photon illumination, photodynamic anticancer treatment is dramatically enhanced by the photothermal effect.

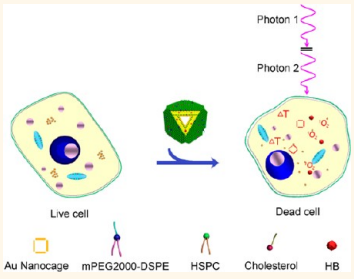

KEYWORDS: gold nanocages · photosensitizer · two-photon photodynamic therapy · photothermal therapy · synergistic effect

To enhance anticancer efficacy and optimize therapy, integration of multimodal treatment strategies leading to synergistic or combined effects is a promising approach.[1,2] Co-assembly of multifunctional agents for systematic therapy has received considerable research interest in cancer treatment.[3−6]

Among all the anticancer treatments, photodynamic therapy (PDT) and photothermal therapy (PTT) involving visible or near-infrared (NIR) light have unique advantages, including remote controllability, low systemic toxicity, and few side effects.[7] The clinically ideal phototherapeutic window for tumors is between 700 and 1100 nm, where the attenuation of light by blood and soft tissues is low, allowing for treating deep-seated tumors. For PDT, light-activated photosensitizers (PSs) can generate reactive oxygen species, such as singlet oxygen ($^1O_2$), free radicals, and peroxides, which can irreversibly damage tumor tissues. Unfortunately, most available PSs, such as hemoporphyrin and phthalocyanine, absorb light energy only over wavelengths shorter than 600 nm, which is a serious drawback for PDT. Thus, great effort has been paid to the design of new PSs or chemical modification of existing ones that have large absorption cross sections in the NIR region.[8−10] For PTT, its implementation relies on the development of photothermal coupling agents. Gold nanostructures, such as nanoshells,[11] nanorods,[12] nanocages,[13−16] assembled gold nanoparticles,[17] and gold nanoshells on polystyrene spheres,[18] represent excellent optical and electronic properties as well as good biocompatibility, enabling their exciting applications in the PTT field. In particular, gold nanocages (AuNCs) exhibit tunable strong scattering and absorption in the NIR transparent window, which enables their use as potential contrast agents and photothermal convertors for cancer diagnosis and therapy.[16,19,20] In addition, AuNCs have hollow interiors and porous walls suitable for encapsulating various drugs.[21,22] Hence, AuNCs uploading special drugs could be expected to serve as intriguing bioconjugates for complex localized NIR therapy.

Up until recently, few reports about dual PDT and PTT for anticancer treatment *in vitro* or *in vivo* concerning the molecular assembled complex have been introduced.

* Address correspondence to jbli@iccas.ac.cn.

Received for review June 14, 2012 and accepted August 29, 2012.

Published online August 29, 2012
10.1021/nn302634m

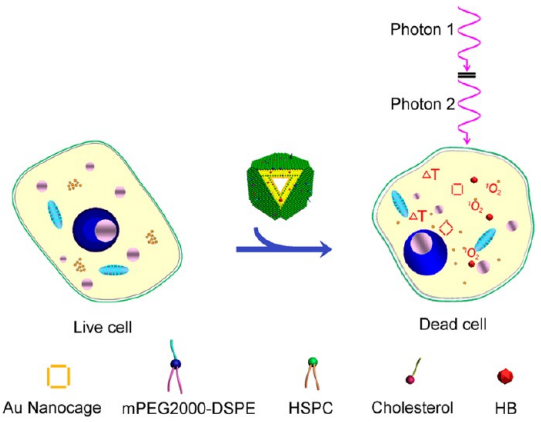

Scheme 1. Schematic illustration of the formulation of lipid-HB-AuNCs and the process of the combinational treatments of two-photon photodynamic/photothermal therapy for suppressing tumor cell growth in a synergistic manner *in vitro*. The hybrid conjugate comprises a gold nanocage as a support core, mixed lipid layers with the incorporation of the two-photon photodynamic therapeutic agent HB, and a hydrophilic PEG shell. After the nanomedicine was co-cultured with and internalized by HeLa cells, the cells were irradiated with a NIR two-photon laser. The simultaneously generated hyperthermia and $^1O_2$ leads to a much enhanced cytotoxicity

For instance, Tian *et al*. demonstrated that the photothermal effect of graphene could be utilized to promote the delivery of Chlorin e6 by mild local heating when exposed to an 808 nm laser, further enhancing PDT efficacy *in vitro* under irradiation by a 660 nm laser.[23] Jang *et al*. confirmed that a gold nanorod−$AlPcS_4$ complex excited by 810 and 670 nm lasers subsequently could reduce tumor growth *in vivo* by 95%.[24] Recently, Khlebtsov *et al*. described composite nanoparticles consisting of a gold−silver nanocage core and a mesoporous silica shell functionalized with the PS Yb-2,4-dimethoxyhematoporphyrin for *in vivo* applications. The fabricated nanocomposites generated singlet oxygen under 630 nm excitation and produced heat under laser irradiation at the plasmon resonance wavelength (750−800 nm).[25] The previous reports showed that treatment with PDT and PTT eventually could not be simultaneously performed due to the incompatibility of photothermal convertors and PSs in the NIR region. How to combine PDT and PTT into a single treatment modality with highly efficiency and compatibility is a great challenge.

In this article, we constructed a nanocomplex by using a lipid-loaded photosensitizer, hypocrellin B (HB), to coat AuNCs and further realized the combined treatment of PDT and PTT for ablation of tumor cells *in vitro*. As illustrated in Scheme 1, first, HB, as a typical two-photon photodynamic therapeutic agent,[26] was reconstituted into hydrogenated soybean phosphatidylcholine, cholesterol, and mPEG2000-distearylphosphatidylethanolamine (mPEG2000-DSPE) constituent mixed lipid vesicles. Then, the obtained vesicles were allowed to spread on the outer surface of the AuNCs. After the lipid-HB-AuNCs were internalized by HeLa cells, a 790 nm NIR two-photon femtosecond pulsed laser was utilized to irradiate the system. With the NIR two-photon irradiation, AuNCs can convert light into heat, and the excited PS can generate reactive oxygen species simultaneously. In this case, PDT and PTT can be combined at the same time for systematic cancer therapy, which will remarkably enhance the treatment efficiency.

RESULTS AND DISCUSSION

By optimizing the experimental conditions, the surface plasmon resonance (SPR) peak of the obtained AuNCs was tuned to about 800 nm to match the central wavelength of the NIR irradiation source. Figure 1a (A) and (C) display scanning electron microscopic (SEM) and transmission electron microscopic (TEM) images of AgNCs as the precursor, which were synthesized through a sulfide-mediated polyol process.[27] Figure 1a (B) and (D) present the typical morphology of AuNCs with small holes at the corners and side faces. The edge length and wall thickness of the prepared nanocages are 45(±5) and 5.0(±0.5) nm, respectively (roughly calculated from 30 AuNCs from their TEM images). On the basis of the results of the inductively coupled plasma mass spectrometry (ICP-MS) analyses, AuNCs as-obtained are composed of 72% Au and 28% Ag in an alloy state (see Supporting Information). Lipid-PS vesicles prepared by a lipid film hydration and membrane extrusion method were obtained, as shown in Figure 1a (E). Dynamic light scattering (DLS) measurement indicates that the mean diameter of the mixed vesicles is about 75 nm (Figure S1), which is similar to the TEM result above.

Lipid-HB vesicles as-prepared were then allowed to decorate the outer surface of AuNCs to form lipid-HB-AuNCs by simply mixing vesicles and AuNC suspensions at 55 °C, a temperature above the phase transition temperature of the mixed liposomes. As shown in Figure 1a (F), AuNCs are surrounded by a continuous soft layer with a low electron density, which might be ascribed to the contribution of lipids. The enlarged TEM image (the inset in Figure 1a (F)) gives the soft layer with an estimated size of around 5 nm, corresponding to the thickness of a lipid bilayer. It is noted that the obtained lipid vesicles have a mean diameter of 75 nm, which will be readily spread on the individual AuNCs. Figure 1b presents the result of energy dispersive X-ray (EDX) analysis of the lipid-HB-AuNCs nanocomposite without the uranyl acetate stain. It gives the elemental components Au, Ag, C, N, O, P, and Cu. The former two elements originate from AuNCs while C, N, O, and P can be ascribed to the composition of the mixed lipid layers and HB accommodated on the surface of the AuNCs. It should be noted that the existence of Cu is from the copper grids. All of these analyses verify that the designed lipid-HB-AuNC nanocomposites are successfully

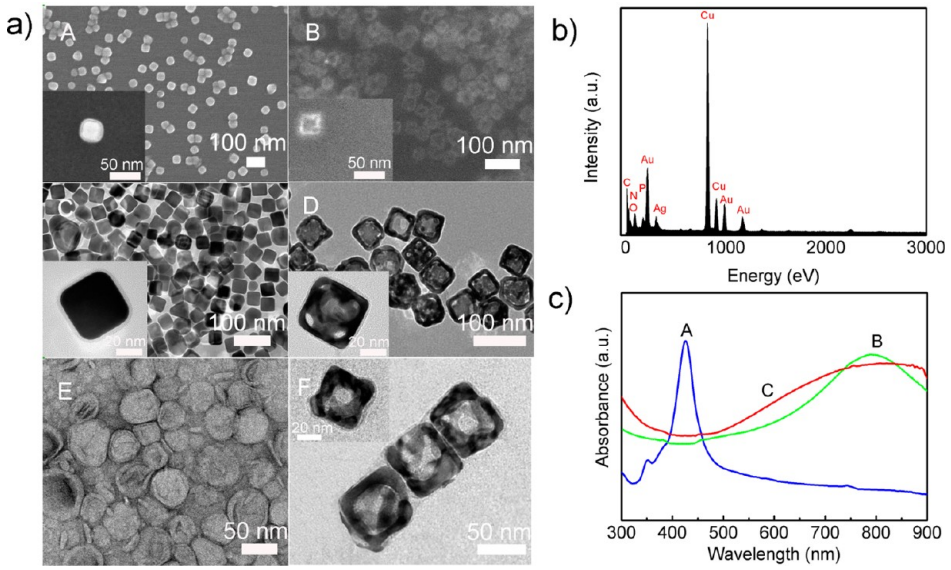

Figure 1. (a) SEM images of (A) AgNCs and (B) AuNCs; TEM images of (C) AgNCs and (D) AuNCs. The insets are relevant images with higher magnification. TEM images of (E) lipid-HB vesicles and (F) lipid-HB-AuNCs as-prepared. They were stained with 1% uranyl acetate. (b) EDX pattern of lipid-HB-AuNCs. (c) UV−vis spectra of the AgNCs (A), AuNCs (B), and lipid-HB-AuNCs (C).

fabricated. The assembled nanocomposites are relatively stable. The experiments showed that there was no observable structural change in the range of physiological solutions including in saline, cell medium, and serum within two weeks of the storage period. This might be ascribed to the surface modification with PEG polymer, which serves as a means of improving nanostructure stability.[28,29]

The SPR feature of the as-prepared particles was explored by UV−vis spectroscopy. Figure 1c shows the characteristic absorption of an aqueous suspension AgNCs (curve A) at about 426 nm and AuNCs (curve B) at about 795 nm. The small variations in the nanocage size, wall thickness, and degree of corner truncation as well as the aggregation of AuNCs may result in the discrepancy of the peak.[19,20] A more broadened plasmon resonance of the lipid-HB-AuNCs (curve C in Figure 1c) can be observed after PEGylated mixed liposomes were spread on the surface of the AuNCs. Considering the results of DLS of AuNCs and lipid-HB-AuNCs presented in Figure S2, the reason for the broadening plasmon resonance might be ascribed to the limited aggregation of the AuNCs after the mixed lipid decoration. It is noted that the resulting absorbance spectrum of lipid-HB-AuNCs (curve C) does not show the major absorption peak of HB. The reason might be ascribed to the much larger absorption cross-section of AuNCs.[13]

In order to confirm that HB is attached to the surface of composite nanoparticles, we carried out the measurements of the fluorescence emission spectra at different pH values, 2, 5, 7, and 13, respectively, according to a published method.[25] The experimental results from the fluorescence emission spectra of AuNCs and lipid-HB-AuNCs in PBS (Figure 2a, black curve and

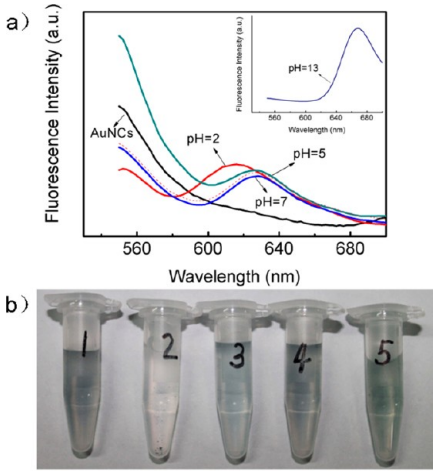

Figure 2. (a) Fluorescence emission spectra of a AuNC suspension at pH 7 and nanocomplex suspensions at pH 2, 5, 7, and 13 after incubation for 12 h, centrifugation, and redispersion. The excitation wavelength is 470 nm. The dashed line shows the initial spectrum of the bioconjugate nanostructure before adjusting the pH values. (b) Photo images of AuNCs (1) and lipid-HB-AuNCs incubated in various solutions at pH 2 (2), 5 (3), 7 (4), and 13 (5) for 12 h, respectively.

bright blue curve) show that the HB's characteristic emission peak appears near 628 nm as excited at 470 nm. This result together with the UV−vis measurement shown in Figure 1c demonstrates that lipid-HB has been successfully decorated on the surface of the AuNCs. Furthermore, the integrity test was performed by spectroscopic examination of the redispersed samples after incubating for 12 h at different pH values. The emission peak of HB at about 628 nm shown in Figure 2a (green and blue curve) confirms the integrity of the obtained particles at pH 5 and 7 after centrifugation and washing. However, the spectrum of the

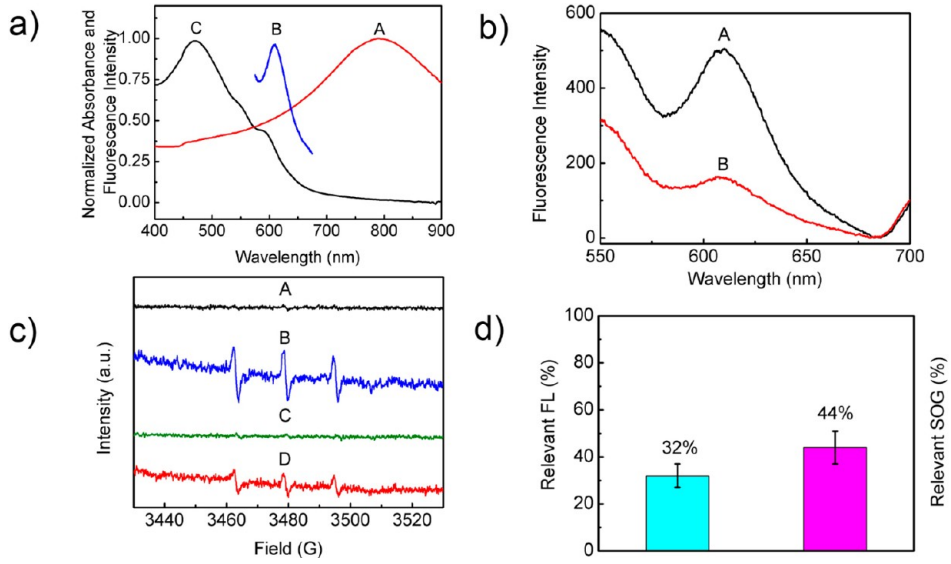

Figure 3. (a) Normalized absorption spectra of AuNCs (A) and lipid-HB (C); normalized fluorescence emission spectrum of lipid-HB (B) excited at 470 nm. (b) Fluorescence emission spectra of lipid-HB (A) and lipid-HB-AuNCs (B) at 140 μM formulated HB equivalent under 470 nm excitation. (c) ESR spectra of the TEMPO adduct in an aqueous solution containing 0.1 M TEMP and 140 μM HB. Lipid-PS for control experiments in which light was omitted (A) and after 60 s irradiation with 532 nm laser (B). Lipid-HB-AuNCs with 0.700 nM AuNCs in which light was omitted (C) and after 60 s irradiation with a 532 nm laser (D). (d) Relative fluorescence intensity (blue) and $^1O_2$ generation (purple) of lipid-HB-AuNCs based on the results of fluorescence and ESR. The measured fluorescence and $^1O_2$ generation of lipid-HB were converted to 100%.

redispersed sample at pH 2 reveals a slight variation (Figure 2a, red curve) in contrast to those at pH 5 and 7. With the nanocomposite in a strong basic solution (pH 13), the emission spectrum gives a remarkable change (inset in Figure 2a). As one can see in Figure 2b, the results of the optic images demonstrate the stability of the redispersed samples at pH 5 and 7 (Figure 2b (3) and (4)). Moreover, the nanocomplex exhibits noticeable aggregation in a strong acid medium (Figure 2b (2)) and severe color conversion in strong base medium (Figure 2b (5)). It could be concluded that the integrity and stability of the nanocomposites in weakly acidic and physiological medium are good, whereas those at extreme low and high pH are poor.

Previous to employing lipid-HB-AuNCs for anticancer treatment, the essential component of the conjugates was evaluated quantitively. UV−vis measurement was carried out to confirm the amount of photosensitizer assembled on the surface of the AuNCs (see Figure S3). Meanwhile, the concentration of AuNCs in the conjugates was clarified by ICP-MS analysis according to the method of Xia's group (see Supporting Information).[30] The final formulation of the nanomedicine is 0.35 nM AuNCs with about 70 μM HB. The as-prepared conjugates were utilized in the following spectroscopy analysis and anticancer treatment *in vitro*.

Retaining the unique optical properties of fluorophores including PSs with plasmonic materials such as gold after nanoscale integration is a long-standing problem because gold nanomaterials can expediently quench the fluorophores.[31−33] Moreover, how to make full use of the law above to alleviate unwelcomed side effects of PDT is another intriguing challenge. In principle, the SPR spectrum of AuNCs (Figure 3a, curve A) partially overlaps with the emission band of lipid-PS (Figure 3a, curve B) when HB was excited at 470 nm, which is the maximum absorbance wavelength (Figure 3a, curve C). Additionally, the absorption cross-section of AuNCs is so large[13] that AuNCs may serve as efficient energy quenchers of excited PSs through their surface energy transfer property when AuNCs and HB were kept in close proximity in our designed nanosystem. With the aim of demonstrating the effect of AuNCs on the PS's photocatalytic activity, the fluorescence and $^1O_2$ generation of lipid-PS before and after being decorated on the surface of AuNCs were investigated (Figure 3b and c). As shown in Figure 3b, the fluorescence inhibitory feature of AuNCs on HB can be quantified by comparing the fluorescence intensity of lipid-PS with that of lipid-HB-AuNCs. More importantly, $^1O_2$ quenching efficiency could be estimated by electron spin resonance (ESR) measurement by means of detecting 2,2,6,6-tetramethyl-4-piperidone (TEMP)-$^1O_2$ spin adduct[34] (see Figure S4), which has a typical triplet ESR signal (Figure 3c). The fluorescence and ESR results show that lipid-HB-AuNCs emit a fluorescence intensity corresponding to 32 ± 5% and $^1O_2$ generation efficiency of 44 ± 7%, compared with those of lipid-PS (Figure 3d). In other words, while lipid-PS is adjacent to the surface of AuNCs, the fluorescence intensity will be reduced and the generation of $^1O_2$ by photocatalysis will be partially inhibited. Clinically, PSs for PDT and two-photon PDT are also sensitive to excitation by UV−vis light; this critical shortcoming results in the

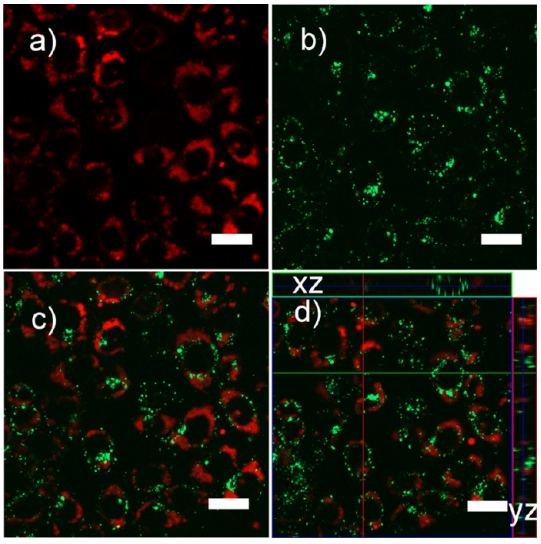

Figure 4. Images of HeLa cells' cellular uptake of lipid-HB-AuNCs after 6 h coculture: (a) one-photon fluorescent image of well-distributed lipid-HB in the whole cytoplasm; (b) two-photon luminescence image of AuNCs scattered in the cytoplasm and on the membrane; (c) the overlapped image; (d) *x*−*y* top view at a given *z* and two other images of the respective *x*−*z* and *y*−*z* side views along the green and red lines. The green and red lines represent the position where the stack is cut to form the *xz* and *yz* sections, respectively. The scale bars are 20 μm.

prolonged sensitivity of patients to sunlight or bright indoor light and can trigger the side effect of damaging normal cells due to the unfavorable biodistribution of the PDT agent. Since the energy transfer between the PS and AuNCs exists, generation of $^1O_2$ will be partly inhibited even under light exposure before the nanocomplex reaches the target spot.[10]

To further determine the intracellular distribution of the complex in tumor cells after cellular endocytosis, lipid-HB-AuNCs and HeLa cells were cocultured at 37 °C for 6 h. Subsequently, free particles outside the plasma membrane were removed and the live cells were imaged by one-photon fluorescence and two-photon luminescence simultaneously at multitrack mode. A one-photon fluorescence image was obtained by scanning the cells with a He−Ne laser at 543 nm, whereas two-photon luminescence was acquired with a femtosecond pulsed laser tuned to 790 nm. The fluorescence and luminescence signals in Figure 4 appear to be strongly localized at the area of treated cells, thus suggesting a substantial degree of interactions between cells and these particles. In detail, the fluorescence from HB excited by a 543 nm laser exhibits a well-distributed red region in the whole cytoplasm, as revealed in Figure 4a. In contrast, in Figure 4b, the green dots scattered in the cytoplasm and on the membrane could be attributed to the two-photon photoluminescence of AuNCs under the plasmon-resonant condition collected in the green channel.[30] Simultaneous co-delivery of AuNCs and HB to the same tumor cell may be beneficial to optimal cooperation in phototherapeutics. Moreover, the overlapped fluorescence microscopy and two-photon luminescence microscopy images (Figure 4c) and three-dimensional image in Figure 4d provide further evidence for endocytosis of nanomedicine according to the distribution of the green and red channels. Taken together, the nanomedicine as-assembled for an adaptive tumor treatment modality could be proposed as follows. Preliminarily, the lipid-HB-AuNCs complex would be supposed to be less phototoxic in the circulatory system even upon light exposure to overcome nonspecific activation of phototoxicity. Then, the nanocomplex would be localized in tumor tissues and further internalized by tumor cells because of a passive targeting effect of nanomaterials. Meanwhile, the tumor cells and tissues could be detected by two-photon photoluminescence with a high signal-to-background ratio and, ultimately, selectively destroyed by an NIR laser in a noninvasive manner by illumination of the detected tumor tissues while minimizing phototoxic damage of the surrounding normal ones. It is worth noticing that, up to now, although a considerable amount of research has been carried out for targeted PS delivery[35] or encapsulation of drugs in hollow structures to overcome unwanted side effects,[36−40] our strategy can be expected to alleviate photosensitizers' unwelcomed side effects resulting from their nontargetability.

Cell mortality can be tuned by a combination of a series of parameters, which has been extensively explored by some research groups. It has been reported that energy input in the system is proportional to concentration of nanoparticles and incident laser power.[41−43] To elucidate the optimized treatment conditions, three factors including concentration of lipid-HB-AuNCs, irradiation exposure time, and power were explored. In a concentration-dependent manner, HeLa cells were seeded in a 96-well plate at 5×10^4 cells/mL per well. Four dosages of nanomedicine were administrated and cocultured with tumor cells under darkness for 6 h, and each well was exposed under 790 nm two-photon laser irradiation at 85.5 pJ per pulse for 300 s. Then, cells were supplemented with fresh culture medium and further incubated for 48 h for apoptosis and necrosis to take place. As shown in Figure 5a, the 3-(4,5-dimethylthiazolyl-2)-2,5-diphenyl tetrazolium bromide (MTT) assay indicates the dose responsive cell death: the more nanomedicine delivered, the more cell death that occurred. Likewise, to find out the threshold NIR irradiation time and power for inducing the most reasonable treatment efficacy, various laser irradiation times and powers were investigated. Practically, lipid-HB-AuNCs with a final concentration of AuNCs of 35.0 pM and HB of 7.0 μM were cocultured with cells by following the same treatment platform mentioned above. As presented in Figure 5b and c, cell viability as a function of irradiation time and

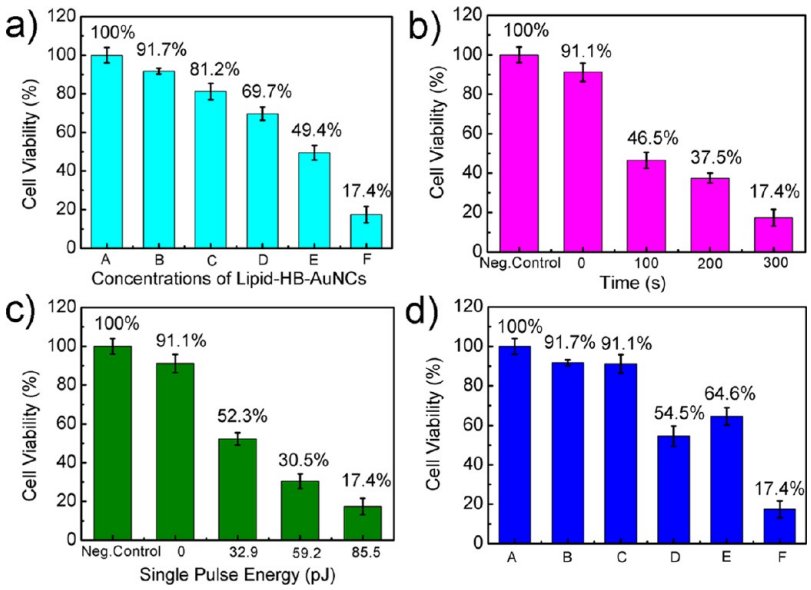

Figure 5. (a) HeLa cell viability *in vitro* measured by MTT assay (n = 3) with dependence on nanomedicine concentration. (A) HeLa cells that were incubated in the absence of agents without irradiation; (B) cells exposed to light alone without any agent; cells cultured with (C) lipid-HB-AuNCs with 4.38 pM AuNCs and 0.88 μM HB; (D) 8.75 pM AuNCs, 1.8 μM HB; (E) 17.5 pM AuNCs, 3.5 μM HB; (F) 35.0 pM AuNCs, 7.0 μM HB for 6 h and then irradiated with the 790 nm two-photon laser at 85.5 pJ per pulse for 300 s. (b) HeLa cell viability *in vitro* measured by MTT assay (n = 3) under irradiation for different times. Lipid-HB-AuNCs with 35.0 pM AuNCs, 7.0 μM HB were cocultured with HeLa cells for 6 h and then irradiated with a 790 nm two-photon laser at 85.5 pJ per pulse for 0, 100, 200, and 300 s, respectively. Cells that were incubated in the absence of agents without irradiation were used as the control group. (c) HeLa cell viability *in vitro* measured by MTT assay (n = 3) at different radiant powers. Lipid-HB-AuNCs with 35.0 pM AuNCs, 7.0 μM HB were cocultured with HeLa cells for 6 h and then irradiated with the 790 nm two-photon laser for 300 s at 0, 32.9, 59.2, and 85.5 pJ per pulse as the experimental groups. Cells that were incubated in the absence of agents without irradiation were used as control groups. (d) HeLa cell viability *in vitro* measured by MTT assay (n = 3) under different conditions: (A) in the absence of agent, without irradiation; (B) without agent, under irradiation of the 790 nm NIR two-photon laser at 85.5 pJ per pulse for 300 s; (C) in the presence of lipid-HB-AuNCs, without irradiation; under the same irradiation above, (D) lipid-PS with 7.0 μM HB; (E) lipid-AuNCs with 35.0 pM AuNCs; (F) lipid-HB-AuNCs with 35.0 pM AuNCs and 7.0 μM HB.

power was plotted, respectively. Increasing time or power means more irradiation energy imposed on the cells, resulting in more intensive cell destruction. It is noteworthy that the cell viability reaches a minimum value under the irradiation conditions of 85.5 pJ per pulse, 300 s. To quantify the synergistically enhanced anticancer effect of the combination of the two treatment approaches, an MTT assay was evaluated. As shown in Figure 5d (A−C), the three control cases yield high cell viabilities of >91.1 ± 4.7%. As a contrast, Figure 5d (D) and (E) show that PDT and PTT lead to cell viabilities of 54.5 ± 5.1% and 64.6 ± 4.4%, respectively. As expected, when the two treatments were combined under a single irradiation, the cell viability was remarkably reduced to 17.4 ± 4.3% (Figure 5d (F)), which is evidently much lower than that by the individual ones.

Furthermore, for the sake of visualizing the tumorigenic cell ablation efficacy and demonstrating the relevant mechanism preliminarily and semiquantitatively *in vitro*, HeLa cells cultured in a glass-bottomed Petri dish were incubated with lipid-HB-AuNCs with final AuNC and HB concentrations of 35.0 pM and 7.0 μM, respectively, for 6 h, followed by illumination with a 790 nm two-photon laser at 85.5 pJ per pulse for 300 s. After a series of combinational treatment with agents and laser, the samples were incubated with a mixture of the nucleic acid-specific dyes acridine orange (AO) and ethidium bromide (EB) following the standard staining protocols[44] and immediately observed by fluorescence microscopy. Assessment of cell viability was carried out by observing fluorescent cell staining: AO enters live cells and gives the nuclei a green fluorescence, while EB is excluded by intact tumor cell membranes but stains the nuclei of dead cells fluorescent orange. In the three control experiments, HeLa cells exhibit no obvious loss of cell viability after NIR irradiation, as do the cells receiving nanomedicine without irradiation (Figure 6a−i). However, all the HeLa cells treated with lipid-HB and irradiation exhibit a bright saffron yellow color, showing late apoptotic or necrotic character (Figure 6j−l). The cell damage may be attributed to generation of $^1O_2$ by a two-photon-induced photodynamic process of HB.[26] For HeLa cells cultured with lipid-AuNCs under irradiation, as presented in Figure 6m−o, the cells around the circular NIR irradiation region are stained green and still remain alive, compared with those located inside the light spot, which are inactive and detached, exhibiting the appearance of necrotic areas by photothermal effects.[45] To further estimate the photothermal

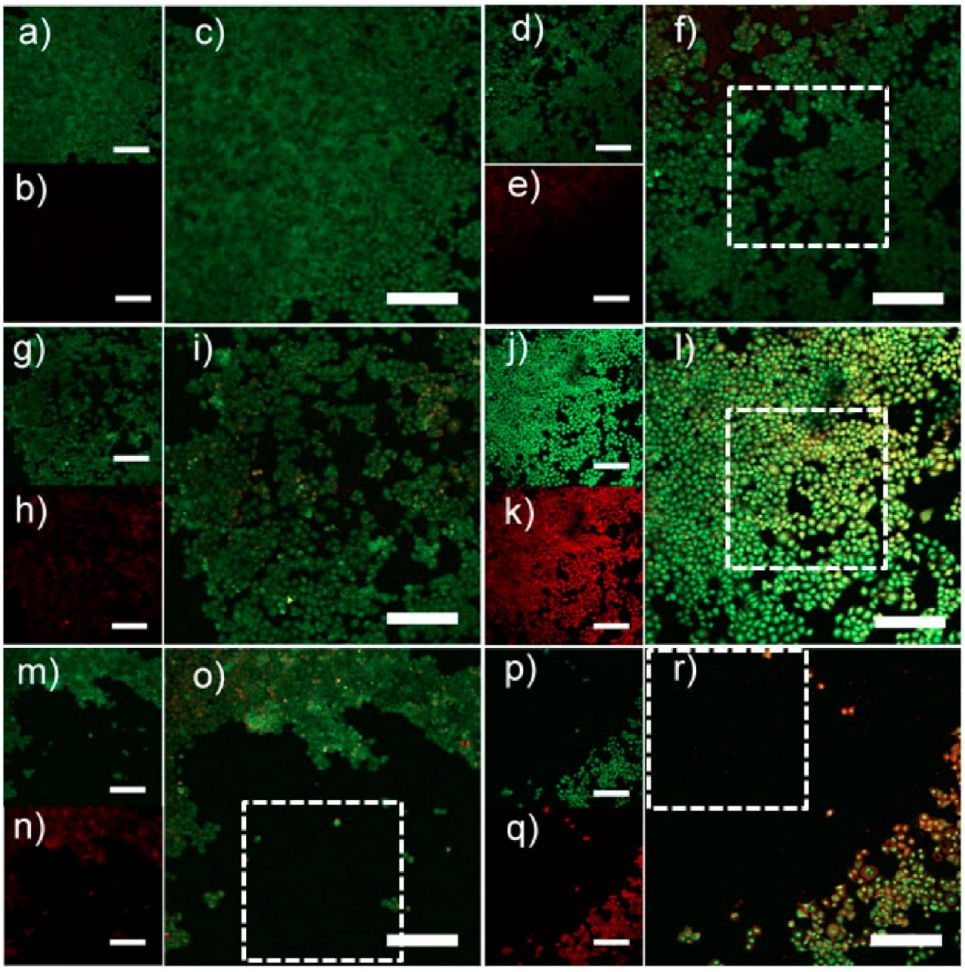

Figure 6. Images of HeLa cells cultured in a glass-bottomed Petri dish incubated with or without various constituent conjugates for 6 h, with or without illumination. After incubating with a mixture of the nucleic acid-specific dyes AO and EB by following standard staining protocols, the samples were observed by fluorescence microscopy through green, red, and their overlayed channels, respectively: (a−c) in the absence of agent, without irradiation; (d−f) without agent, under irradiation of a 790 nm NIR two-photon laser at 85.5 pJ per pulse for 300 s; (g−i) in the presence of lipid-HB-AuNCs, without irradiation; under the same irradiation above, (j−l) lipid-HB with 7.0 μM HB; (m−o) lipid-AuNCs with 35.0 pM AuNCs; (p−r) lipid-HB-AuNCs with 35.0 pM AuNCs and 7.0 μM HB. It should be noted that (c), (f), (i), (l), (o), and (r) are the corresponding overlapped images. The area inside the marked white line is the corresponding laser scanning region. (NOTE: The real area under irradiation is larger than the marked spot because of the Gaussian distribution of light.) The scale bars are 200 μm.

effect *in situ*, HeLa cells incubated with lipid-AuNCs were illuminated by scanning the same area repetitively and quickly with a 790 nm laser. During the process, ballooning bulges could be observed, which is in good agreement with the results reported by Xia's group,[45] who explained that it is an indication of membrane blebbing resulting from temperature increase (see red and blue arrows in Figure S5). In contrast, for the case of HeLa cells cultured with lipid-HB-AuNCs under irradiation, not only does a necrotic area exist but also the viability of cells around the circular NIR-irradiated region is compromised, indicating enhanced cell membrane damage[46] (Figures 6p−r). It is notable that the image exhibits a quarter of the necrotic area, suggesting the absolute necrotic area of the combined treatment (about 2.0 mm^2) is definitely larger than that of PTT treatment alone (about 0.5 mm^2). The result vividly proves the combined PDT and PTT treatment regime by two-photon therapy can dramatically enhance the possibility of destroying tumor cells *in vitro*, compared to that by using each single method.

From the tumor cellular mortality ratio, one can see a significant synergistic therapeutic effect. This may be ascribed to a positive Arrhenius-type enhancement of the photosensitization reactions resulting from hyperthermia derived from PTT.[47] To demonstrate the above mechanism, we have carried out the relevant experiments. First, the temperature changes in the lipid-AuNC suspensions under the two-photon irradiation were investigated. As shown in Figure 7a, the temperature increase in the simplified lipid-AuNCs system shows a positive concentration dependence.[43] Then another experiment was proposed to clarify the temperature-dependent photoreaction. In detail, the reaction of $^1O_2$ generated by lipid-HB with 9,10-diphenylanthracene (DPA) was studied in H_2O at different

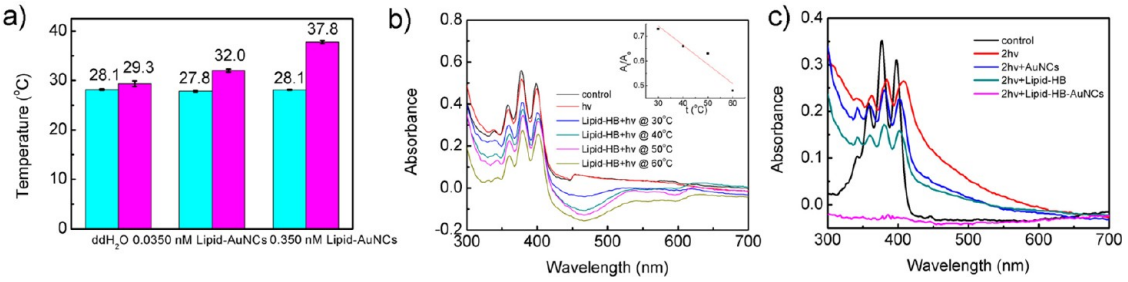

Figure 7. (a) Plots of temperatures in H_2O and two suspensions of lipid-AuNCs recorded by a thermocouple before and after NIR two-photon illumination (85.5 pJ per pulse for 300 s, 790 nm). In two suspensions, the concentrations of AuNCs are 0.0350 and 0.350 nM. (b) UV−vis spectra of DPA in H_2O−DMSO without irradiation (black curve); in H_2O−DMSO with irradiation upon 480 nm one-photon excitation for 300 s (red curve); together with lipid-HB under the same irradiation above at 30 (blue curve), 40 (green curve), 50 (pink curve), and 60 °C (yellow curve), respectively. The final concentration of HB in the formulation is 70 μM. The irradiation source is a 150 W Xe lamp, equipped with filters to isolate a narrow spectral region around 480 nm. A_t/A_0 represents the ratio of remnant DPA after irradiation at the designated temperature. (c) UV−vis spectra of DPA in H_2O−DMSO without irradiation (black curve); in H_2O−DMSO with irradiation upon 790 nm two-photon excitation at 85.5 pJ per pulse for 300 s (red curve); together with AuNCs (blue curve), lipid-HB (green curve), or lipid-HB-AuNCs (pink curve) under the same irradiation as above. In the nanomedicine, the final concentrations of AuNCs and HB are about 0.350 nM and 70 μM.

temperatures ranging from 30 to 60 °C. The oxidation of DPA by $^1O_2$ (Figure S6) could be observed by the absorbance decrease of DPA at 376 nm.[48] This result suggests that the rates of the photosensitization reaction increase with an increase in temperature (Figure 7b). Moreover, based on the above results, photobleaching of DPA by $^1O_2$ generated by lipid-HB-AuNCs under two-photon excitation was explored. As illustrated in Figure 7c, an obvious absorbance decrease of DPA at 376 nm in the presence of lipid-HB-AuNCs is observed after two-photon irradiation at 85.5 pJ per pulse for 300 s (pink curve), compared to that of the DPA solution with or without irradiation (Figure 7c, red curve and black curve). To demonstrate the synergistic influence of hyperthermia on PDT, we have done control experiments for the irradiation of DPA with AuNCs or lipid-HB. As expected, relatively less photobleaching of DPA was observed under both conditions (Figure 7c, blue curve and green curve), indicating a positive Arrhenius-type enhancement of the photosensitization reactions induced by the photothermal effect.[49−53] Thus we conclude that with the aid of the two-photon technique, the combined treatment of PDT and PTT exhibits an obvious advantage. It has been reported that the highly localized plasmonic field of AuNPs and their aggregates can enhance the formation of reactive oxygen species from PS.[54] Arrhenius-type enhancement of the photosensitization can be expected to be another efficient strategy to generate elevated reactive oxygen species, which is definitely the key for highly efficient PDT for cancer treatment. Moreover, one-off administration and irradiation based on the two-photon technique is convenient for integration of different approaches to facilitate the combined treatment.

CONCLUSIONS

In summary, we constructed a lipid-HB-AuNCs complex for two-photon photothermal/photodynamic cancer therapy *in vitro*. The assembly of photosensitizer and photothermal transducer and the utilization of two-photon techniques results in one-off administration and irradiation for antitumor treatment. The present method is supposed to lower the PSs' negative effect in the unnecessary nontargeted area. The relevant experiments display an obviously synergistic anticancer efficiency in the NIR region by coupling PDT and PTT. Thus such an assembled complex may become a more effective system for cancer therapy.

EXPERIMENTAL SECTION

Chemicals and Reagents. Ethylene glycol, $AgNO_3$, $Na_2S\cdot 9H_2O$, $HAuCl_4\cdot 3H_2O$, anhydrous chloroform, acetone, and ethanol were obtained from Beijing Chemical Reagent Co., China. Polyvinylpyrrolidone with average $M_r \approx 55\,000$ and 2,2,6,6-tetramethyl-4-piperidone were from Sigma-Aldrich. Hydrogenated soybean phosphatidylcholine (HSPC) and mPEG2000-distearylphosphatidylethanolamine (mPEG2000-DSPE) were purchased from Nippon Fine Chemical Co., Ltd., Japan. Cholesterol was bought from Avanti Polar Lipids (Alabaster, AL, USA). Hypocrellin B (HB) was kindly provided by Zhao's group. Acridine orange (AO) and ethidium bromide (EB) were obtained from Beijing BioDee Biotechnology Corporation Ltd., China. 9,10-Diphenylanthracene (DPA) was from Alfa Aesar China (Tianjin) Co., Ltd. 3-(4,5-Dimethylthiazolyl-2)-2,5-diphenyl tetrazolium bromide (MTT) was purchased from Amresco. Penicillin, streptomycin, Dulbecco's modified Eagle medium (DMEM), and fetal bovine serum (FBS) were obtained from Invitrogen. All other materials were commercially available and used as received unless otherwise mentioned. The water with a resistivity of 18.2 MΩ·cm, used throughout the experiment, was purified with a Milli-Q system from Millipore Co., USA.

Preparation of Mixed Liposomes with and without Photosensitizer. Mixed liposomes composed of HSPC, cholesterol, and mPEG2000-DSPE with a molar ratio of about 2:1:0.16 were prepared by a lipid film hydration and membrane extrusion method.[55] In detail, stock solutions of HSPC (1.0 mg), cholesterol (0.25 mg), and mPEG2000-DSPE (0.31 mg) in the presence or

absence of 50 μg of HB in anhydrous chloroform were mixed in a vitreous vial. The mixture was blown dry with N_2 and further dried under vacuum for 24 h. After incubation and gentle stirring in 1.0 mL of H_2O for 2 h at 37 °C, the lipid mixture was then extruded to form liposomes at 55 °C by following the instruction from Avanti Polar Lipids, Inc.

Fabrication of Lipid-AuNCs and Lipid-HB-AuNCs. AuNCs were prepared by a galvanic replacement reaction between Ag nanocubes serving as the sacrificial templates and $HAuCl_4$ by following a method reported by Xia's group.[27] To fabricate lipid-AuNCs and lipid-HB-AuNCs, the as-prepared 1.0 mL of lipid and lipid-PS vesicles were added to the AuNC dispersion (0.21 nM, 0.5 mL) and gently stirred at 55 °C for 1 h, respectively. The obtained dispersions were centrifuged at 10 000 rpm for 20 min, respectively. After the conjugates were washed three times with H_2O or PBS, both lipid-coated AuNCs were resuspended in 300 μL of H_2O or PBS, respectively, and used as soon as possible.

Characterization. The morphologies of the samples were examined by a Hitachi S-4800 SEM working at 15 kV. TEM was conducted with a JEOL 2011 transmission electronic microscope working at 200 kV. The elemental components were analyzed by an EDX analyzer (Phoenix) as the TEM accessory. A Hitachi U-3010 spectrophotometer was used to record the UV−vis spectra. In addition, the mean diameter and size distribution were documented by a phase analysis light scattering technique (Zetasizer Nano, Malvern). Fluorescence emission spectra were obtained by a F-4500 fluorescence spectrophotometer (Hitachi). The ESR spectra were measured by using a Bruker model ESP 300 spectrometer operating at room temperature. Au and Ag content were determined by ICP-MS (PerkinElmer). One-photon and two-photon fluorescence images were obtained by a two-photon laser scanning microscope (Carl Zeiss LSM 510 Meta). A mode-locked femtosecond Ti:sapphire laser (Coherent Mira-900, USA) tuned to 790 nm with a repetition rate of 76 MHz and pulse width of 130 fs was used as the two-photon illumination source.

ESR Measurements. The spin trap agent TEMP reacts with $^1O_2$ forming stable nitroxyl radical spin adduct TEMPO, which produces a typical triplet ESR signal.[34] Photoinduced ESR spectra were obtained by mixing 0.1 M TEMP with lipid-HB or lipid-HB-AuNCs suspension to reach a final HB concentration of 140 μM. Samples were then injected into quartz capillaries designed specially for ESR analysis and directly irradiated inside the cavity of the ESR spectrometer with a Q-switched Nd:YAG nanosecond laser apparatus. The exciting wavelength was 532 nm. Parameter settings: microwave power, 10.09 mW; frequency, 9.8 GHz; time constant, 40.96 ms; scan width, 100 G. The ESR signals of TEMPO generated by lipid-HB or lipid-HB-AuNCs in the presence of TEMP without irradiation were collected as controls.

Endocytosis Study of Lipid-HB-AuNCs. With regard to the endocytosis study, 5×10^4 cells/mL HeLa cells were grown in 35 mm glass-bottom Petri dishes, supplemented with culture medium at a concentration to allow 90% confluence in 24 h. Then, lipid-HB-AuNCs with a final AuNC concentration of 35.0 pM were delivered. After incubating with the conjugates at 37 °C for 6 h, the cells were washed three times with PBS, and then 1 mL of culture medium was supplemented into the glass-bottom Petri dishes. Finally, the cells were immediately observed with a 0.55 numerical aperture oil immersion 63× objective, and individual images were taken along their *z*-axis at 1 μm intervals. Fluorescence and luminescence images were taken by multitrack mode: HB excited by the 543 nm laser was detected mainly in the red channel through an emission filter at 565−615 nm, while two-photon photoluminescence of AuNCs was collected mainly in the green channel through an emission filter at 500−550 nm when excited by the 790 nm laser.

Anticancer Treatments *in Vitro*. HeLa cells were cultured in DMEM and 10% FBS supplemented with 1% penicillin and streptomycin at 37 °C in 5% CO_2, 70% humidity environment, reseeded every 2−4 days to maintain subconfluency. Anticancer treatments *in vitro* under different conditions were carried out. The MTT assay was used to evaluate the relevant cell viabilities. Survival of untreated cells was set as 100%, and that of test cells was expressed as a percentage of untreated cells. Data are shown as (mean ± the standard error) from three independent experiments performed in triplicate.

AO/EB Staining of HeLa Cells for Observation of Necrotic or Apoptotic Areas. After lipid-HB-AuNCs as well as other drugs were cocultured with HeLa cells for 6 h, the experimental groups and control groups were illuminated with the 790 nm two-photon laser (85.5 pJ per pulse, 300 s) under an objective (20×, NA 0.55) with the continuous scanning mode (1 frame/s). After irradiation, 10 μL of 50 μg mL^{-1}AO and EB mixed dye solution in PBS was added to each Petri dish and cocultured with cells under darkness for 20 min at room temperature. Soon afterward, the cells were washed five times with PBS to remove the unreacted dye and detached cells before observing by confocal laser scanning microscopy. Then, HeLa cells were observed with a 0.55 numerical aperture 10× objective. Emission of AO was collected mainly in the green channel through an emission filter at 500−550 nm when excited by a 488 nm Ar^+ laser. EB excited by a 543 nm He−Ne laser was detected mainly in the red channel through an emission filter at 565−615 nm. All the fluorescent images were collected at the same setting.

Photothermal Measurements. For concentration-depended photothermal measurements, a homemade thermocouple that allows thermal detection with an accuracy of 0.01 °C was used. Samples (500 μL) were placed in a sealed quartz cuvette (4.5 × 1.0 × 0.5 cm) and then irradiated from the top by *z*-axis scanning at steps of 7.5 μm/s (85.5 pJ per pulse for 300 s, 790 nm). Temperature increase was immediately measured along the scanning cross section, and a total of three replicates were conducted for each sample. Lipid-AuNCs with AuNC concentrations of 0.0350 and 0.350 nM were measured as experimental groups and H_2O as the control group.

Temperature-Dependent Singlet Oxygen Generation by Lipid-HB. In a typical measurement, the sample was prepared by mixing 630 μL of lipid-HB in H_2O with 70 μL of DPA stock solution in DMSO into a sealed quartz cuvette as mentioned above before placing it in a water bath at the designated temperature (30, 40, 50, and 60 °C). The final concentration of HB is 70 μM, and that of DPA is 55 μM. After irradiation for 300 s, the suspension was then taken out for UV−vis spectral measurement (Note: the UV−vis spectrum of lipid-PS with 70 μM HB in H_2O/DMSO mixed solution was recorded as the corresponding baseline). The irradiation source is a 150 W Xe lamp with a narrow spectral region around 480 nm.

DPA Bleaching Study for AuNCs, Lipid-HB, and Lipid-HB-AuNCs under Two-Photon Excitation. The sample was prepared by mixing 630 μL of AuNCs, lipid-HB, or lipid-HB-AuNCs in H_2O with 70 μL of DPA stock solution in DMSO, respectively. The final concentration of DPA was 55 μM. For AuNCs, the final concentration was 0.350 nM. For lipid-HB, the final concentration of HB was 70 μM. For lipid-HB-AuNCs, the final concentrations of AuNCs and HB were 0.350 nM and 70 μM. Two-photon excitation at 790 nm (85.5 pJ per pulse, 300 s) was conducted by enabling a laser beam through a sealed quartz cuvette containing 700 μL of suspensions. After irradiation for 300 s, in the case of AuNCs or lipid-HB-AuNCs, the sample was centrifugated and the supernatant was then taken out for UV−vis spectral measurement. For lipid-HB, the suspension was measured directly (Note: in this case, the UV−vis spectrum of lipid-HB with 70 μM HB in H_2O/DMSO mixed solution was recorded as the corresponding baseline).

Conflict of Interest: The authors declare no competing financial interest.

Acknowledgment. We thank Prof. Jingquan Zhao for kindly providing HB. We also thank Dr. Luru Dai for helpful discussions. We gratefully acknowledge financial support from the National Nature Science Foundation of China (Project No. 91027045) and National Basic Research Program of China (973 Program 2009CB930101).

Supporting Information Available: The Supporting Information file contains UV−vis and ICP-MS measurements to determine the amount of essential component of the conjugates; phototoxicity effect of lipid-AuNCs on HeLa cells; anticancer treatment *in vitro* under different conditions; dynamic light scattering size distributions of mixed liposomes, AuNCs, and

lipid-HB-AuNCs; mechanisms of two methods for singlet oxygen detection. This material is available free of charge *via* the Internet at http://pubs.acs.org.

REFERENCES AND NOTES

1. Greco, F.; Vicent, M. J. Combination Therapy: Opportunities and Challenges for Polymer-Drug Conjugates as Anticancer Nanomedicines. *Adv. Drug Delivery Rev.* **2009**, *61*, 1203–1213.
2. Lane, D. Designer Combination Therapy for Cancer. *Nat. Biotechnol.* **2006**, *24*, 163–164.
3. Sengupta, S.; Eavarone, D.; Capila, I.; Zhao, G.; Watson, N.; Kiziltepe, T.; Sasisekharan, R. Temporal Targeting of Tumour Cells and Neovasculature with a Nanoscale Delivery System. *Nature* **2005**, *436*, 568–572.
4. Zhang, L. F.; Radovic-Moreno, A. F.; Alexis, F.; Gu, F. X.; Basto, P. A.; Bagalkot, V.; Jon, S. Y.; Langer, R. S.; Farokhzad, O. C. Co-delivery of Hydrophobic and Hydrophilic Drugs From Nanoparticle-aptamer Bioconjugates. *ChemMedChem* **2007**, *2*, 1268–1271.
5. Sun, T. M.; Du, J. Z.; Yao, Y. D.; Mao, C. Q.; Dou, S.; Huang, S. Y.; Zhang, P. Z.; Leong, K. W.; Song, E. W.; Wang, J. Simultaneous Delivery of siRNA and Paclitaxel *via* a "Two-in-One" Micelleplex Promotes Synergistic Tumor Suppression. *ACS Nano* **2011**, *5*, 1483–1494.
6. Liu, H. Y.; Chen, D.; Li, L. L.; Liu, T. L.; Tan, L. F.; Wu, X. L.; Tang, F. Q. Multifunctional Gold Nanoshells on Silica Nanorattles: a Platform for the Combination of Photothermal Therapy and Chemotherapy with Low Systemic Toxicity. *Angew. Chem., Int. Ed.* **2011**, *50*, 891–895.
7. Phillips, D. Light Relief: Photochemistry and Medicine. *Photochem. Photobiol. Sci.* **2010**, *9*, 1589–1596.
8. Velusamy, M.; Shen, J. Y.; Lin, J. T.; Lin, Y. C.; Hsieh, C. C.; Lai, C. H.; Lai, C. W.; Ho, M. L.; Chen, Y. C.; Chou, P. T.; *et al.* A New Series of Quadrupolar Type Two-Photon Absorption Chromophores Bearing 11, 12-Dibutoxydibenzo[*a*,*c*]-phenazine Bridged Amines; Their Applications in Two-Photon Fluorescence Imaging and Two-Photon Photodynamic Therapy. *Adv. Funct. Mater.* **2009**, *19*, 2388–2397.
9. Ogawa, K.; Kobuke, Y. Design of Two-Photon Absorbing Materials for Molecular Optical Memory and Photodynamic Therapy. *Org. Biomol. Chem.* **2009**, *7*, 2241–2246.
10. Bobo, M. G.; Mir, Y.; Rouxel, C.; Brevet, D.; Basile, I.; Maynadier, M.; Vaillant, O.; Mongin, O.; Desce, M. B.; Morere, A.; *et al.* Mannose-Functionalized Mesoporous Silica Nanoparticles for Efficient Two-Photon Photodynamic Therapy of Solid Tumors. *Angew. Chem., Int. Ed.* **2011**, *50*, 11425–11429.
11. Wu, G. H.; Mikhailovsky, A.; Khant, H. A.; Fu, C.; Chiu, W.; Zasadzinski, J. A. Remotely Triggered Liposome Release by Near-Infrared Light Absorption *via* Hollow Gold Nanoshells. *J. Am. Chem. Soc.* **2008**, *130*, 8175–8177.
12. Park, J. H.; Maltzahn, G. V.; Ong, L. L.; Centrone, A.; Hatton, T. A.; Ruoslahti, E.; Bhatia, S. N.; Sailor, M. J. Cooperative Nanoparticles for Tumor Detection and Photothermally Triggered Drug Delivery. *Adv. Mater.* **2010**, *22*, 880–885.
13. Chen, J.; Wiley, B. J.; Li, Z. Y.; Campbell, D. J.; Saeki, F.; Cang, H.; Au, L.; Lee, J.; Li, X.; Xia, Y. Gold Nanocages: Engineering Their Structure for Biomedical Applications. *Adv. Mater.* **2005**, *17*, 2255–2261.
14. Skrabalak, S.; Chen, J. Y.; Sun, Y. G.; Lu, X. M.; Au, L.; Cobley, C. M.; Xia, Y. N. Gold Nanocages: Synthesis, Properties, and Applications. *Acc. Chem. Res.* **2008**, *41*, 1587–1595.
15. Chen, J. Y.; Yang, M. X.; Zhang, Q.; Cho, E. C.; Cobley, C. M.; Kim, C. H.; Glaus, C.; Wang, L. V.; Welch, M. J.; Xia, Y. Gold Nanocages: A Novel Class of Multifunctional Nanomaterials for Theranostic Applications. *Adv. Funct. Mater.* **2010**, *20*, 3684–3694.
16. Xia, Y.; Li, W. Y.; Cobley, C. M.; Chen, J.; Xia, X.; Zhang, Q.; Yang, M. X.; Cho, E. C.; Brown, P. K. Gold Nanocages: From Synthesis to Theranostic Applications. *Acc. Chem. Res.* **2011**, *44*, 914–924.
17. Wang, S. T.; Chen, K. J.; Wu, T. H.; Wang, H.; Lin, W. Y.; Ohashi, M.; Chiou, P. Y.; Tseng, H. R. Photothermal Effects of Supramolecularly Assembled Gold Nanoparticles for the Targeted Treatment of Cancer Cell. *Angew. Chem., Int. Ed.* **2010**, *49*, 3777–3781.
18. Liu, H. Y.; Chen, D.; Tang, F. Q.; Du, G. J.; Li, L. L.; Meng, X. W.; Liang, W.; Zhang, Y. E.; Teng, X.; Li, Y. Photothermal Therapy of Lewis Lung Carcinoma in Mice Using Gold Nanoshells on Carboxylated Polystyrene Spheres. *Nanotechnology* **2008**, *19*, 455101.
19. Chen, J. Y.; Wang, D. L.; Xi, J. F.; Au, L.; Siekkinen, A.; Warsen, A.; Li, Z. Y.; Zhang, H.; Xia, Y. N.; Li, X. D. Immuno Gold Nanocages with Tailored Optical Properties for Targeted Photothermal Destruction of Cancer Cells. *Nano Lett.* **2007**, *7*, 1318–1322.
20. Chen, J. Y.; Glaus, C.; Laforest, R.; Zhang, Q.; Yang, M. X.; Gidding, M.; Welch, M. J.; Xia, Y. N. Gold Nanocages as Photothermal Transducers for Cancer Treatment. *Small* **2010**, *6*, 811–817.
21. Yavuz, M. S.; Cheng, Y. Y.; Chen, J. Y.; Cobley, C. M.; Zhang, Q.; Rycenga, M.; Xie, J. W.; Kim, C. H.; Song, K. H.; Schwartz, A. G.; *et al.* Gold Nanocages Covered by Smart Polymers for Controlled Release with Near-Infrared Light. *Nat. Mater.* **2009**, *8*, 935–939.
22. Moon, G. D.; Choi, S. W.; Cai, X.; Li, W. Y.; Cho, E. C.; Jeong, U.; Wang, L. V.; Xia, Y. N. A New Theranostic System Based on Gold Nanocages and Phase-Change Materials with Unique Features for Photoacoustic Imaging and Controlled Release. *J. Am. Chem. Soc.* **2011**, *133*, 4762–4765.
23. Tian, B.; Wang, C.; Zhang, S.; Feng, L. Z.; Liu, Z. Photothermally Enhanced Photodynamic Therapy Delivered by Nano-graphene Oxide. *ACS Nano* **2011**, *5*, 7000–7009.
24. Jang, B.; Park, J.; Tung, C.; Kim, I.; Choi, Y. Gold Nanorod-Photosensitizer Complex for Near-Infrared Fluorescence Imaging and Photodynamic/Photothermal Therapy *in Vivo*. *ACS Nano* **2011**, *5*, 1086–1094.
25. Khlebtsov, B.; Panfilova, E.; Khanadeev, V.; Bibikova, O.; Terentyuk, G.; Ivanov, A.; Rumyantseva, V.; Shilov, I.; Ryabova, A.; Loshchenov, V. Enhanced Release of Small Molecules from Near-Infrared Light Responsive Polymer-Nanorod Composites. *ACS Nano* **2011**, *5*, 7077–7089.
26. Liu, J.; Zhao, Y. W.; Zhao, J. Q.; Xia, A. D.; Jiang, L. J.; Wu, S.; Ma, L.; Dong, Y. Q.; Gu, Y. H. Two-photon Excitation Studies of Hypocrellins for Photodynamic Therapy. *J. Photochem. Photobiol. B* **2002**, *68*, 156–164.
27. Skrabalak, S. E.; Au, L.; Li, X. D.; Xia, Y. N. Facile Synthesis of Ag Nanocubes and Au Nanocages. *Nat. Protoc.* **2007**, *2*, 2182–2190.
28. Wang, L. S.; Wu, L. C.; Lu, S. Y.; Chang, L. L.; Teng, I. T.; Yang, C. M.; Ho, J. A. Biofunctionalized Phospholipid-Capped Mesoporous Silica Nanoshuttles for Targeted Drug Delivery: Improved Water Suspensibility and Decreased Nonspecific Protein Binding. *ACS Nano* **2010**, *4*, 4371–4379.
29. Barreto, J. A.; Malley, W.; Kubeil, M.; Graham, B.; Stephan, H.; Spiccia, L. Nanomaterials: Applications in Cancer Imaging and Therapy. *Adv. Mater.* **2011**, *23*, H18–H40.
30. Au, L.; Zhang, Q.; Cobley, C. M.; Gidding, M.; Schwartz, A. G.; Chen, J. Y.; Xia, Y. N. Quantifying the Cellular Uptake of Antibody-Conjugated Au Nanocages by Two-Photon Microscopy and Inductively Coupled Plasma Mass Spectrometry. *ACS Nano* **2010**, *4*, 35–42.
31. Fan, C. H.; Wang, S.; Hong, J. W.; Bazan, G. C.; Plaxco, K. W.; Heeger, A. J. Beyond Superquenching: Hyper-efficient Energy Transfer from Conjugated Polymers to Gold Nanoparticles. *Proc. Natl. Acad. Sci. U. S. A.* **2003**, *100*, 6297–6301.
32. Jin, Y. D.; Gao, X. H. Plasmonic Fluorescent Quantum dots. *Nat. Nanotechnol.* **2009**, *4*, 571–576.
33. Griffin, J.; Singh, A. K.; Senapati, D.; Rhodes, P.; Mitchell, K.; Robinson, B.; Yu, E.; Ray, P. C. Size- and Distance-dependent Nanoparticle Surface-Energy Transfer (NSET) Method for Selective Sensing of Hepatitis C Virus RNA. *Chem.—Eur. J.* **2009**, *15*, 342–351.
34. Dzwigaj, S.; Pezerat, H. Singlet Oxygen-Trapping Reaction as a Method of $^1O_2$ Detection: Role of Some Reducing Agents. *Free Radical Res.* **1995**, *23*, 103–115.
35. Olivo, M.; Bhuvaneswari, R.; Lucky, S. S.; Dendukuri, N.; Soo-Ping Thong, P. Targeted Therapy of Cancer Using

Photodynamic Therapy in Combination with Multifaceted Antitumor Modalities. *Pharmaceuticals* **2010**, *3*, 1507–1529.
36. Amstad, E.; Reimhult, E. Nanoparticle Actuated Hollow Drug Delivery Vehicles. *Nanomedicine* **2012**, *7*, 145–164.
37. Yan, X. H.; Li, J. B.; Möhwald, H. Templating Assembly of Multifunctional Hybrid Colloidal Spheres. *Adv. Mater.* **2012**, *24*, 2663–2667.
38. Skirtach, A. G.; Yashchenok, A. M.; Möhwald, H. Encapsulation, Release and Applications of LbL Polyelectrolyte Multilayer Capsules. *Chem. Commun.* **2011**, *47*, 12736–12746.
39. Peteiro-Cartelle, J.; Rodríguez-Pedreira, M.; Zhang, F.; Gil, P. R.; Mercato, L. L.; Parak, W. J. One Example on How Colloidal Nano- and Microparticles could Contribute to Medicine. *Nanomedicine* **2009**, *4*, 967–979.
40. Bédard, M. F.; Sadasivan, S.; Sukhorukov, G. B.; Skirtach, A. Assembling Polyelectrolytes and Porphyrins into Hollow Capsules with Laser-Responsive Oxidative Properties. *J. Mater. Chem.* **2009**, *19*, 2226–2233.
41. Javier, A. M.; Pino, P.; Bedard, M. F.; Ho, D.; Skirtach, A. G.; Sukhorukov, G. B.; Plank, C.; Parak, W. J. Photoactivated Release of Cargo from the Cavity of Polyelectrolyte Capsules to the Cytosol of Cells. *Langmuir* **2008**, *24*, 12517–12520.
42. Skirtach, A. G.; Javier, A. M.; Kreft, O.; Köhler, K.; Alberola, A. P.; Möhwald, H.; Parak, W. J.; Sukhorukov, G. B. Laser-Induced Release of Encapsulated Materials inside Living Cells. *Angew. Chem., Int. Ed.* **2006**, *45*, 4612–4617.
43. Skirtach, A. G.; Dejugnat, C.; Braun, D.; Susha, A. S.; Rogach, A. L.; Parak, W. J.; Möhwald, H.; Sukhorukov, G. B. The Role of Metal Nanoparticles in Remote Release of Encapsulated Materials. *Nano Lett.* **2005**, *5*, 1371–1377.
44. Parks, D. R.; Bryan, V. M.; Oi, V. T.; Herzenberg, L. A. Antigen-Specific Identification and Cloning of Hybridomas with a Fluorescence-Activated Cell Sorter. *Proc. Natl. Acad. Sci. U. S. A.* **1979**, *76*, 1962–1966.
45. Tong, L.; Cobley, C. M.; Chen, J. Y.; Xia, Y. N.; Cheng, J. X. Bright Three-Photon Luminescence from Gold/Silver Alloyed Nanostructures for Bioimaging with Negligible Photothermal Toxicity. *Angew. Chem., Int. Ed.* **2010**, *49*, 3485–3488.
46. Chen, B.; Xu, Y.; Agostinis, P.; Witte, P. Synergistic Effect of Photodynamic Therapy with Hypericin in Combination with Hyperthermia on Loss of Clonogenicity of RIF-1 Cells. *Int. J. Oncol.* **2001**, *18*, 1279–1285.
47. Gottfried, V.; Kimel, S. Temperature Effects on Photosensitized Processes. *J. Photochem. Photobiol. B* **1991**, *8*, 419–430.
48. Yu, C. L.; Chen, S.; Zhang, M. H.; Shen, T. Spectroscopic Studies and Photodynamic Actions of Hypocrellin B in Liposomes. *Photochem. Photobiol.* **2001**, *73*, 482–488.
49. Orenstein, A.; Kostenich, G.; Kopolovic, Y.; Babushkina, T.; Malik, Z. Enhancement of ALA-PDT Damage by IR-Induced Hyperthermia on A Colon Carcinoma Model. *Photochem. Photobiol.* **1999**, *69*, 703–707.
50. Chen, B.; Roskams, T.; Witte, P. Enhancing the Antitumoral Effect of Hypericin-Mediated Photodynamic Therapy by Hyperthermia. *Laser Surg. Med.* **2002**, *31*, 158–163.
51. Henderson, B. W.; Waldow, S. M.; Potter, W. R. Interaction of Photodynamic Therapy and Hyperthermia: Tumor Response and Cell Survival Studies after Treatment of Mice *in Vivo*. *Cancer Res.* **1985**, *45*, 6071–6077.
52. Yanase, S.; Nomura, J.; Matsumura, Y.; Nagata, T.; Fujii, T.; Tagawa, T. Synergistic Interaction of 5-aminolevulinic Acid-Based Photodynamic Therapy with Simultaneous Hyperthermia in an Osteosarcoma Tumor Model. *Int. J. Oncol.* **2006**, *29*, 365–373.
53. Kah, J.; Wan, R.; Wong, K.; Mhaisalkar, S.; Sheppard, C.; Olivo, M. Combinational Treatment of Photothermal Therapy Using Gold Nanoshells with Conventional Photodynamic Therapy to Improve Treatment Efficacy: An *in Vitro* Study. *Laser Surg. Med.* **2008**, *40*, 584–589.
54. Oo, M.; Yang, Y. M.; Hu, Y.; Gomez, M.; Du, H.; Wang, H. J. Gold Nanoparticle-Enhanced and Size-Dependent Generation of Reactive Oxygen Species from Protoporphyrin IX. *ACS Nano* **2012**, *6*, 1939–1947.
55. Cao, Z. H.; Tong, R.; Mishra, A.; Xu, W. C.; Wong, G.; Cheng, J. J.; Lu, Y. Reversible Cell-Specific Drug Delivery with Aptamer-Functionalized Liposomes. *Angew. Chem., Int. Ed.* **2009**, *48*, 6494–6498.